# Sheffield Hallam University

# Synthesis and characterisation of Li11RE18M4O39−δ: RE = Nd or Sm; M = Al, Co or Fe

CHEN, Yao-Chen, REEVES-MCLAREN, Nik, TAN, Chaou C., BINGHAM, Paul, FORDER, Sue and WEST, Anthony R.

Available from Sheffield Hallam University Research Archive (SHURA) at:

http://shura.shu.ac.uk/11333/

This document is the author deposited version. You are advised to consult the publisher's version if you wish to cite from it.

## Published version

## Repository use policy

# Synthesis and characterisation of $Li_{11}RE_{18}M_4O_{39-\delta}$ :

# RE = Nd or Sm; M = Al, Co or Fe

Yao-Chang Chen,[1] Nik Reeves-McLaren,[1] Chaou C Tan,[1] Paul A Bingham,[2] Susan D Forder[2] and Anthony R West*,[1]

[1]Department of Materials Science and Engineering, University of Sheffield, Mappin Street, Sheffield, S1 3JD, UK

[2] Materials and Engineering Research Institute, Sheffield Hallam University, City Campus, Howard Street, Sheffield, S1 1WB, UK

**Abstract**

Four new phases of general formula, $Li_{11}RE_{18}M_4O_{39-\delta}$ : REM = NdAl, NdCo, SmCo, SmFe, have been synthesised and characterised. The NdAl phase, and probably the others, is isostructural with the NdFe analogue, but some cation disorder and partial site occupancies prevent full structural refinement of powder neutron diffraction data. The NdCo phase also forms a solid solution with variable Li content (and charge compensation by either oxygen vacancies or variable transition metal oxidation state). The NdAl phase is a modest conductor of $Li^+$ ions whereas the other three phases are electronic conductors, attributed to mixed valence of the transition metal ions. Subsolidus phase diagrams for the systems $Li_2O – Nd_2O_3 – Al_2O_3,$ 'CoO' have been determined and an additional new phase, $LiCoNd_4O_8$, which appears to have a $K_2NiF_4$ – related superstructure, identified.

**Introduction**

There has been considerable interest in recent years in oxide phases that contain lithium, a rare earth cation and one or more transition metals.[1-12] This is in large part due to their often interesting magnetic or electrical properties; for example, perovskite-structured $Li_{3x}La_{2/3-x}TiO_3$[11] and Li-stuffed garnet phases such as $Li_7La_3Zr_2O_{12}$[12] exhibit high levels of Li-ion conductivity at ambient temperatures and are leading solid electrolyte candidates for the next generation of all solid-state Li battery applications.

Another family of lithium – rare earth - transition metal oxides of significant interest that has been discovered by Battle and co-workers has the general formula $Li_xRE_{18}M_5O_{39}$, where RE = La, Pr, Nd; M = Ti, Mn, Fe, Co, Ru, Rh, though not all RE/M combinations have been studied.[3,5-9] Most reports gave the Li content as $x = 8$, but our recent investigation[10] of the pseudoternary phase diagram for the $Li_2O$-$Nd_2O_3$-$Fe_2O_3$ system, with careful attention to processing conditions to avoid lithium loss during synthesis, yielded the ternary phase, $Li_{11}Nd_{18}Fe_4O_{39-\delta}$, which clearly belongs to the same structural family as the above phases but has both a different RE:M ratio and Li content. The particular problems in working with these materials are that (i) it can be difficult to avoid lithium loss during synthesis and therefore, uncertainties over phase stoichiometry exist and (ii) structure determination using powder diffraction methods, linked to confirmation of phase stoichiometry, is complicated by mixed and/or partial occupancy of some Li and/or transition metal sites.

Notwithstanding complexities and uncertainties over composition(s) and detailed site occupancies of these phases, their main structural features are clear.[3,5-9] Taking $Li_{11}Nd_{18}Fe_4O_{39-\delta}$ as an example, the structure contains intersecting <111>

chains of alternating, face-sharing Fe(2a)-$O_6$ or Fe(8e)-$O_6$ octahedra and Li(16i)-$O_6$ trigonal prisms. The chains are surrounded by a network of fully-occupied Nd(24k)-$O_9$ and Nd(12f)-$O_7$ polyhedra.

The main differences between the various structure reports concern the 2a, 8e and 16i sites occupied by transition metals and Li. In some reports, there is single ion occupancy of particular sites but in others, multiple cations are disordered over the same set of sites; in our study[10] of $Li_{11}Nd_{18}Fe_4O_{39-\delta}$, a new lithium site (24k) with occupancy 1/6 was proposed. In all cases, however, the RE and most oxygen sites are fully occupied; oxygen deficiency in certain cases is accommodated by one particular oxygen site, O(4), 48l. Given the number of crystallographic sites over which there is uncertainty, together with details of phase stoichiometry, it is likely that solving remaining problems in the crystal chemistry of these interesting phases will require use of single crystal diffraction data.

Our approach to the study of materials in this family of phases is to avoid loss of lithium during synthesis so that the resulting compositions are the same as the starting compositions (after elimination of volatile gases). This is achieved by (i) immersing pellets of the reaction mixtures in powders of the same composition that had already been reacted ('buffering') and (ii) phase diagram determination, utilising a wide range of starting compositions, in which the layout of resulting subsolidus compatibility triangles helps to pinpoint and confirm the compositions of individual phases which must lie at the corners of the various compatibility triangles[10].

This general approach requires self-consistent results to be obtained on heating a range of compositions until no further changes are observed, at which point thermodynamic equilibrium is presumed to be attained[10]. It is very different to the

open synthesis of target compositions to which an excess of $Li_2CO_3$ is added to compensate for expected lithium loss: samples are heated until essentially single phase materials are obtained and the compositions are deduced or confirmed by follow-on neutron diffraction studies[3,5-9].

In this paper, we report results on the synthesis, preliminary structural studies and electrical properties of several new analogues in this family of general formula, $Li_{11}RE_{18}M_4O_{39-\delta}$: RE = Nd, Sm; M = Al, Co, Fe and the determination of equilibrium ternary phase diagrams for two systems, $Li_2O$-$Nd_2O_3$-$Al_2O_3$,'CoO'. In addition to the new phases which have Li content of 11 in the general formula, a new solid solution, $Li_{11-x}Nd_{18}Co_4O_{39-\delta}$ is reported. Unit cell data and phase stoichiometries were characterised using powder X-ray diffraction, XRD, scanning electron microscopy, SEM with energy dispersive spectroscopy, EDS for elemental analysis and $^{57}Fe$ Mössbauer spectroscopy; electrical properties were measured using impedance spectroscopy, IS.

**Experimental**

Solid state synthesis of a wide range of compositions in the systems $Li_2O$-$RE_2O_3$-$M_2O_3$ (RE = Nd, Sm; M = Al, Co, Fe) was carried out using high purity $Li_2CO_3$ and appropriate metal oxides as starting reagents. Reagents were dried and weighed out in stoichiometric amounts to give ~ 5 g batch sizes. These were ground together with acetone using an agate mortar and pestle for ~15 min, dried and heated in Au foil boats at 400 °C for 2 h followed by 700 °C for 12 h to initiate loss of $CO_2$ and commence reaction. Samples were cooled, crushed and divided into two portions; pellets were pressed, uniaxially, from one portion and covered with the remaining

powder; the whole assemblage was returned to the furnace and heated for various times and temperatures in the range 800 - 950 °C. This buffering procedure was designed to avoid $Li_2O$ loss from the pelleted samples during heating; final firing schedules were determined by trial and error to find appropriate conditions to achieve equilibrium, as indicated by no further change in the various phase assemblages with either additional heating time or increased temperature. At these reaction temperatures, the products were thermodynamically stable in air and the actual reaction temperatures were not critical other than to achieve complete reaction within 1-2 days. The only change in nature of the reaction product that may be anticipated at other temperatures is a small reduction in oxygen stoichiometry, especially at higher temperatures; any oxygen loss would be charge-balanced by reduction in transition metal valence leading to the possibility of increased electronic conduction (there is some evidence for this; see later).

For phase analysis, a Siemens D5000 X-ray diffractometer, Co $K\alpha_1$ radiation, $\lambda$ = 1.7890 Å was used with measurements over the $2\theta$ range 5 - 90 °. Phase identification and indexing used the WinX$^{POW}$ software package. For accurate lattice parameter measurements, data were collected using a STOE STADI P transmission X-ray diffractometer with a linear position sensitive detector and Mo $K\alpha_1$ radiation, $\lambda$ = 0.7093 Å.

Room temperature $^{57}$Fe Mössbauer spectra were collected relative to $\alpha$–Fe over the velocity range ± 4 mm s$^{-1}$ using a constant acceleration spectrometer with a 25 mCi source of $^{57}$Co in Rh. The spectra were fitted satisfactorily with three broadened Lorentzian paramagnetic doublets using the Recoil analysis software package.

Fe, Co and rare earth contents of grains within pelleted samples were obtained semi-quantitatively using EDS in a JEOL 6400 (JEOL Ltd, Tokyo, Japan) SEM operating at 20 kV and a working distance ~ 14 – 17 mm.  The overall transition metal and rare earth contents of samples after reaction should be the same as the starting compositions, but EDS analysis provided a check on sample homogeneity and the compositions of individual grains, which would not be obtained by whole-sample, elemental analysis

Electrical property measurements used an impedance analyzer HP 4192A with frequency range 5 Hz to 10 MHz and temperature range 25-500 °C in air. In order to obtain pellets with sufficient mechanical strength for them to be handled and assembled into the conductivity jig, pellets covered with sacrificial powder were sintered by heating at 950 °C for 24 h. Au paste was applied on opposite pellet faces as electrodes; this was decomposed and hardened by heating to 800 °C for 2 h. An *ac* voltage of ~ 100 mV was applied during measurements. Data were corrected for the sample geometric factor and for the stray capacitance of the sample jig.

**Results**

*The ternary phase diagram $Li_2O$-$Nd_2O_3$-$Al_2O_3$*

A total of 12 compositions was prepared, with results summarised in Table 1. Samples were given a final heat treatment at 950 °C for 24 h in air, and were considered to be at thermodynamic equilibrium as no further changes to the products occurred on subsequent heating. From these results, the phase diagram shown in Fig.

1 was constructed. Results are fully consistent with the identity and location of the 8 compatibility triangles that are shown.

The phase diagram shows one ternary compound, $Li_{11}Nd_{18}Al_4O_{38.5}$. For simplicity, and especially for materials whose composition may be uncertain, this phase and similar phases in other systems are labelled as phase Y. Composition 1 in the phase diagram contained phase Y with trace amounts of $NdAlO_3$ and $Nd_2O_3$ after reaction at 950 °C for 24 h, as shown in Fig. 2. The secondary phases may be associated with a small amount of lithium loss during synthesis, consistent with the phase diagram results. Phase Y was readily identified by comparison of its XRD pattern with that of $Li_{11}Nd_{18}Fe_4O_{39-\delta}$, Fig. 2 and was indexed on a cubic unit cell, space group $Pm\bar{3}n$, $a = 11.8880(1)$ Å; fully indexed data for this and the other new phases have been submitted for inclusion in the Powder Diffraction File. The similarity of the diffraction patterns suggested that this new phase, Y, is isostructural with $Li_{11}Nd_{18}Fe_4O_{39-\delta}$; composition 12, corresponding to the formula $Li_8Nd_{18}Al_5O_{38.5}$, was not phase-pure and contained significant amounts of secondary phases, Table 1.

Preliminary structural studies on $Li_{11}Nd_{18}Al_4O_{38.5}$ were carried out using ND data; results are summarised in Supplementary Tables 1 and 2. The phase is essentially isostructural with the Fe analogue, but uncertainties remain associated with a large amount of structural disorder and partial site occupancies. Thus: the Al,Li(1) and (2) sites contain a disordered mixture of Al and Li; the Li(3) and O(4) sites are only partially occupied; the Li(1) – Li(3) distance, 1.83(1)Å, is too short for both sites to be occupied simultaneously; the Al(1) – O distances are similar to those expected for tetrahedral Al, whereas the coordination is nominally octahedral. Similar questions were raised concerning the structure of the Fe analogue [10] and have also been encountered in structure refinements of other transition metal – rare earth

combinations within this family of materials. It was hoped that the simple composition of the Al phase, without the possibility of variable oxidation state cations and therefore variable oxygen content, would lead to less structural uncertainty, but that is not the case.

### The system $Li_2O$-$Nd_2O_3$-'$CoO$'

A total of 21 compositions was prepared in this system with results listed in Supplementary Table 3. All compositions were given a final heat treatment at 950 °C for 12 h in air. From these results, the ternary phase diagram, Fig. 3, was constructed. Powder XRD highlighted two new findings of note: first, as well as phase Y, a limited series of phase Y solid solution of general formula $Li_{11-x}Nd_{18}Co_4O_{39-\delta}$ formed over the range $0 \leq x \leq 2.9$, with no evidence of any secondary phase formation, Supplementary Fig. 1. From Fig 3, the secondary phase would be $LiCoNd_4O_8$ which is in close proximity to the solid solutions and should, therefore, be readily detected by XRD. Refined lattice parameters decreased with increasing lithium vacancy concentration from ~ 11.8575 Å ($x = 0.00$) to ~ 11.8495 Å ($x = 2.90$, *i.e.* $Li_{8.1}Nd_{18}Co_4O_{39-\delta}$); however, the changes were too small to test whether any deviations from Vegard's law occurred. The solid solutions are characterised most obviously by a reduction in Li content but this must be charge compensated, either by creation of oxygen vacancies or by oxidation of Co: it is assumed that Co is present primarily in the +3 valence state in the parent $Li_{11}Nd_{18}Co_4O_{39-\delta}$ phase; therefore, either some $Co^{4+}$ or

oxygen vacancies may form in the solid solutions.  Further work is required to establish the charge compensation details.

Second, the XRD and phase diagram results show the formation of a previously-unreported ternary compound, $LiCoNd_4O_8$, Fig. 4, together with a small amount of $NdCoO_3$ present as an impurity phase. Most of the XRD data were indexed on a body-centred tetragonal, $K_2NiF_4$-type unit cell with $a = 3.7242(4)$ Å, $c = 12.293(3)$ Å; several weak unindexed peaks were observed which could perhaps be attributed to a supercell based on the $K_2NiF_4$ structural model; further work is needed to fully characterise this new phase.

An additional check on several compositions of the phase Y solid solution series $Li_{11-x}Nd_{18}Co_4O_{39-\delta}$ to determine the Nd:Co ratio was made using EDS. Average values obtained from analyses of 10 randomly-selected spots for each sample are as follows, NdCo, x=0, Nd:Co = 4.4(1); x=2.07, Nd:Co = 4.2(3); x = 2.48, Nd:Co = 4.1(2); x = 2.9, Nd:Co = 4.4(5). They are all within 2 esds of the expected ratio 4.5:1 and are significantly different from the ratio 3.6:1 which would be expected for compositions such as $Li_8Nd_{18}Fe_5O_\delta$.

## $Li_{11}Sm_{18}M_4O_{39-\partial}$

XRD data for Sm-based Y phases, $Li_{11}Sm_{18}M_4O_{39-\delta}$: M = Co, Fe, Supplementary Fig. 2, were collected for specimens slow-cooled from 850 °C; these showed $Li_{11}Sm_{18}Fe_4O_{39-\delta}$ to be single-phase, while $Li_{11}Sm_{18}Co_4O_{39-\delta}$ contained trace amounts of $LiCoO_2$ and $Sm_2O_3$. These new phases were indexed using cubic unit cells: for $Li_{11}Sm_{18}Fe_4O_{39-\delta}$, $a = 11.8486(2)$ Å; for $Li_{11}Sm_{18}Co_4O_{39-\delta}$, $a = 11.7297(2)$

Å. The expected rare earth:transition metal ratios in both were 4.5:1, and EDS

analyses, Sm:Fe = 4.1(1); Sm:Co = 4.2(1), were in reasonable agreement, within 2

esds.

The $^{57}$Fe Mössbauer spectrum, Fig. 5, of $Li_{11}Sm_{18}Fe_4O_{39-\delta}$ was satisfactorily

fitted using three Lorentzian doublets; the extracted spectral parameters (centre shift

($\delta$), quadrupole splitting ($\Delta$) and half-width, half-maximum (HWHM) line-width

($\Gamma/2$)) are given in Table 2. The results are similar to those reported previously for

$Li_8Nd_{18}Fe_4O_{39-\delta}$ and similar compounds [4-10]. For $Li_{11}Sm_{18}Fe_4O_{39-\delta}$ the largest doublet

had a centre-shift of 0.28 mm s$^{-1}$, a low quadrupole splitting of 0.10 mm s$^{-1}$ and a fitted

area of 68%, all consistent with high-spin $Fe^{3+}$. The second doublet, with centre shift

of -0.28mm s$^{-1}$, quadrupole splitting of 0.36 mm s$^{-1}$ and a fitted area of 22%, is

consistent with low-spin $Fe^{4+}$. The third doublet had a centre-shift of 0.10 mm s$^{-1}$, a

quadrupole splitting of 1.10 mm s$^{-1}$ and a fitted area of 10%; this is indicative of high-

spin $Fe^{3+}$ on an additional, third, crystallographic site.

*Electrical properties*

**$\underline{Li_{11}Nd_{18}Al_4O_{38.5}}$**

The electrical properties of a pellet of $Li_{11}Nd_{18}Al_4O_{38.5}$ (density = 68%) were

measured by IS over the temperature range 25 to 500 °C, Fig. 6. The impedance

complex plane plots, $Z''$ vs $Z'$, showed, Fig. 6(a), a slightly broadened arc at high

frequencies. This arc was attributed to the sample bulk because[13] (i) corresponding

M''/Z'' spectra, (b), showed single, partially overlapping peaks, (ii) high frequency

capacitance data, (c), had approximate values in the range 2-5 pFcm$^{-1}$ and (iii) plots of

log Y' vs log f, (d), showed a frequency-independent plateau attributed to the bulk conductivity with a dispersion to higher conductivities attributed to Jonscher power law behaviour[14] at higher frequencies and lower temperatures.

From these data, it is clear that the bulk response of the sample was being measured, but the response showed departures from the ideality expected for a single parallel RC element. By inclusion of a constant phase element, CPE, in the equivalent circuit, Fig. 7(a), a good fit to the experimental data was obtained, (b-e). The CPE represents the dispersions seen in both (i) the Y' data at high frequencies/low temperatures and (ii) the higher frequency of the two dispersions seen in the C' data; $C_1$ represents the limiting, frequency-independent capacitance of the sample, expected at high frequencies, which is not modelled using a CPE alone. $R_1$ represents the total conductivity of the sample, which equals the bulk conductivity since there was no detectable grain boundary impedance. Values of the fitting parameters at 580K are listed in Fig. 7; these show that parameter CPE1-P, commonly referred to as n, with a value of 0.64, is largely responsible for the non-ideality in the impedance data at high frequencies.

At lower frequencies and higher temperatures, a second component is seen in the impedance data as a low frequency spike in the complex plane plot, Fig. 6(a) inset, and a low frequency dispersion in log C'/log f, (c). The C' data reach a value of *e.g.* $10^{-6}$ Fcm$^{-1}$ at 704 K and 10 Hz, indicative of a thin layer capacitance associated with ion blocking at the sample-electrode interface. From these capacitance data, and observation of the low frequency 'electrode spike' in Fig. 6(a), the species responsible for the conductivity appears to be ionic rather than electronic. The 'electrode spike', Fig. 6(a), is mainly composed of a linear region inclined at 45° to the real Z' axis and is a Warburg impedance in which diffusion of electroactive species towards/away

from the sample-electrode interface controls the impedance at lower frequencies. Such a feature is characteristic of both oxide ion conductors and $Li^+$ ion conductors at high temperatures. With oxide ion conductors, there is usually an additional, intermediate frequency impedance associated with the $O^{2-}/O_2$ charge transfer at the sample-electrode interface. This is not seen in Fig. 6 and we believe that the conducting species are $Li^+$ ions.

Bulk conductivity data were extracted, either from the low frequency intercepts of the high frequency arc in the $Z^{"}$ vs $Z^{'}$ plot, Fig. 6(a), or from frequency-independent plateaux in log $Y'$ vs log f, Fig. 6(d), and are plotted in Arrhenius format in Fig. 8. The data are non-linear with approximate activation energies at high and low temperature of 1.51(7) and 0.85(3) eV, respectively. The data are reversible on heat-cool cycles which indicates that there is no change in sample composition, such as possible Li loss, during the impedance measurements.

$Li_{11}Nd_{18}Al_4O_{38.5}$ is, therefore, a modest $Li^+$ ion conductor with a conductivity ~ $1x10^{-6}$ $Scm^{-1}$ at 300 °C and a low temperature activation energy, 0.85(3) eV that is considerably higher than that of the best $Li^+$ ion conductors. The change in activation energy at higher temperature may represent a change from extrinsic to intrinsic $Li^+$ ion conduction and/or the involvement of an extra set of $Li^+$ ions in the conduction process in which the activation energy has components due to both the creation of mobile $Li^+$ ions by freeing them from trapped sites and their subsequent migration.

## $Li_{11-x}Nd_{18}Co_4O_{39-\delta}$

The electrical properties of four members of the phase Y: Nd,Co solid solutions (density~ 63%) were measured by IS over the temperature range 25 to 250 °C. The impedance complex plane plots, Supplementary Fig. 3(a), show two semicircles; for the same data, combined Z" and M" spectroscopic plots, (b), show overlapping Z" / M" peaks at high frequencies which are attributed to the sample bulk. A second Z" peak at lower frequencies does not have an associated M" peak (when data are plotted on linear M" scales). The spectroscopic plots of capacitance, C', (c) show two plateaux at ~ (0.5-1) x $10^{-12}$ Fcm$^{-1}$ and ~ (1-2) x$10^{-11}$ Fcm$^{-1}$ which are attributable to bulk and grain boundary constriction impedances. Bulk conductivities plotted in Arrhenius format, Fig. 9, are linear with activation energy ~ 0.30 eV. No low frequency spike, which might indicate Li$^+$ ionic conductivity, was observed; these compositions are therefore likely to be modest electronic conductors, e.g. ~ 1x$10^{-6}$ Scm$^{-1}$ at ~ 362 K.

## $Li_{11}Sm_{18}M_4O_{39-\delta}$ :M = Co, Fe

Pellets with M= Fe and Co were heated at 850 and 750 °C, respectively. Both samples, with pellet density ~ 60 %, showed similar electrical behaviour to $Li_{11}Nd_{18}Co_4O_{39-\delta}$. Impedance complex plane plots, not shown, consisted of two partially overlapping two semicircles but with no evidence of a low frequency electrode spike; spectroscopic plots of capacitance, C', showed two plateaux at ~$10^{-12}$ and ~ $10^{-11}$ Fcm$^{-1}$.

The Arrhenius plots, Figure 10, showed two parallel lines with similar activation energy, ~ 0.46 eV for the bulk and grain boundary conductivities of the Fe phase; the similar activation energies are good evidence[15] that the grain boundary resistance is a constriction impedance associated with poor pellet sintering and relatively low pellet density. The two impedance arcs were less-well resolved for the Co phase and the bulk and grain boundary resistances were more similar, Fig 10, with activation energies of ~ 0.34 and 0.45 eV. The Sm analogue phases are therefore, also, modest electronic conductors.

**Discussion**

A combination of buffered synthesis to avoid lithium loss, phase diagram determination and SEM/EDS, provides strong evidence that the general stoichiometry of phases in this family, of which 4 new members are reported here, is $Li_{11}RE_{18}M_4O_{39-\delta}$. This is rather different to that of a large number of similar phases reported in the literature [3,5-9] which have smaller Li contents, 8, but higher M content, 5. However, one of our new phases, REM = NdCo, also forms a range of lithium-deficient solid solution, with a Li content as small as 8.1 in the general formulae. The possibility clearly exists that other phases within this family may have variable stoichiometry, which may, in part, help to explain the reported stoichiometry discrepancies associated with the Li content.

Crystallographic studies to determine phase stoichiometries are of limited use in this family of phases due to uncertainties over site occupancies. Thus, in recent studies of the NdFeAl, NdFeGa and LaFeIn analogues[16], the 8$e$ and 16$i$ sites are assumed to have full occupancy but contain 2 or 3 different cations; in the sites with 3

cations, the occupancy of one cation was fixed and that of the other two was refined within the constraint of overall full site occupancy. Given the possibility that vacancies may also be present in these sites, determination of cation stoichiometries by refinement would appear to involve considerable uncertainty.

The stoichiometry of the NdAl analogue reported here has an oxygen content of 38.5, assuming standard valences of 3+ for Nd and Al. The 48$l$ site of oxygen O(4) has been identified to have partial occupancy[15] in the phases with 39 oxygens per formula unit and may therefore be the site with reduced oxygen occupancy in the NdAl analogue. The oxygen contents of the transition metal-containing analogues NdCo and NdFe are not known, but for NdFe are likely to be different from that in NdAl. Thus, the Mössbauer data for SmFe (the analogue for NdFe) show evidence for mixed valence $Fe^{3+/4+}$ which should be linked to the oxygen content. For NdCo, the stoichiometric phase may have the same oxygen content as NdAl if Co is present as $Co^{3+}$, but one possible charge compensation mechanism to account for Li deficiency in the NdCo solid solutions involves oxygen vacancy creation. For these reasons, we give oxygen contents in general terms as 39-$\delta$ but without specifying the values of $\delta$.

The NdAl phase shows a modest level of $Li^+$ ion conductivity which may be associated with partially occupied sites in the crystal structure. These could be the new, 24$k$ sites reported in the structure of the NdFe analogue[10]. The other three phases are all modest electronic conductors which is attributed to the probable mixed valence of the transition metal components. However, their conductivities are several orders of magnitude higher than that of NdAl and so, it is possible that they also have a small level of $Li^+$ ion conductivity which is much less than that of the electronic conductivity and is not detected by the impedance measurements.

Captions

Table 1. Results of sample heat treatment in the $Li_2O$-$Nd_2O_3$-$Al_2O_3$ system

Table 2. Fitted spectral parameters for room temperature Mössbauer spectrum of $Li_{11}Sm_{18}Fe_4O_{39}$

Supplementary Table 1. Results of Rietveld refinement of $Li_{11}Nd_{18}Al_4O_{38.5}$.

Supplementary Table 2. Selected bond lengths (Å) in $Li_{11}Nd_{18}Al_4O_{38.5}$.

Supplementary Table 3. Results of sample heat treatment in the $Li_2O$-$Nd_2O_3$-'CoO' system

Figure 1. The ternary subsolidus phase diagram of the $Li_2O$-$Nd_2O_3$-$Al_2O_3$ system

Figure 2. The XRD patterns of $Li_{11}Nd_{18}Al_4O_{38.5}$ and $Li_{11}Nd_{18}Fe_4O_{39}$; ◆: $LiAlO_2$ and ■: $Nd_2O_3$

Figure 3. Subsolidus phase diagram for the system $Li_2O$-$Nd_2O_3$-'CoO'

Figure 4. XRD pattern of $LiCoNd_4O_8$; ●: $NdCoO_3$.

Figure 5. Fitted Mössbauer spectrum of $Li_{11}Sm_{18}Fe_4O_{39-\delta}$ obtained at room temperature

Figure 6. IS data for $Li_{11}Nd_{18}Al_4O_{38.5}$ at 580 K and 704 K ; pellet density ~68 %; (a) impedance, Z*, complex plane plots, (b) –Z", M" spectroscopic plots, (c) log C' / log f, and (d) log Y'/log f.

Figure 7. (a) equivalent circuit for the bulk response; log-log spectroscopic plots of the real and imaginary parts of (b) $Y^*$, (c) $Z^*$, (d) $C^*$, and (e) $M^*$ for $Li_{11}Nd_{18}Al_4O_{38.5}$ at 580 K; fitted parameters are tabulated

Figure 8. Arrhenius plot of bulk conductivity of $Li_{11}Nd_{18}Al_4O_{38.5}$.

Figure 9. Arrhenius plot of the bulk conductivity of $Li_{11-x}Nd_{18}Co_4O_{39-x/2}$ : $x = 0$ - ~ 2.9

Figure 10. Arrhenius plot of bulk and grain boundary conductivities of SmFe and SmCo phases

Supplementary Figure 1. XRD patterns of the solid solution $Li_{11-x}Nd_{18}Co_4O_{39-\delta}$ : $x = 0$- ~ 2.9

Supplementary Figure 2. XRD patterns of $Li_{11}RE_{18}M_4O_{39-\delta}$:RE = Nd, Sm; M=Co,Fe:  ■ $LiCoO_2$ and ◆: $Sm_2O_3$

Supplementary Figure 3. IS data for the solid solution, $Li_{11-x}Nd_{18}Co_4O_{39-x/2}$:$x = 0$ and 2.9.

Table 1. Results of sample heat treatment in the $Li_2O$-$Nd_2O_3$-$Al_2O_3$ system

| Composition | Molar ratio $Li_2O$ : $Nd_2O_3$: $Al_2O_3$ | Phases present** |
|---|---|---|
| 1 ($Li_{11}Nd_{18}Al_4O_{38.5}$) | 0.333 : 0.546 : 0.121 | Y and a trace of $NdAlO_3$, $Nd_2O_3$ |
| 2 | 0.33 : 0.60 : 0.07 | Y, $LiNdO_2$ and $Nd_2O_3$ |
| 3 | 0.43 : 0.50 : 0.07 | Y, $LiNdO_2$ and a trace of $Li_2O$ |
| 4 | 0.50 : 0.40 : 0.10 | Y, $Li_5AlO_4$ and a trace of $Li_2O$ |
| 5 | 0.50 : 0.30 : 0.20 | Y, $Li_5AlO_4$ and $LiAlO_2$ |
| 6 | 0.30 : 0.50 : 0.20 | Y, $LiAlO_2$ and $NdAlO_3$ |
| 7 | 0.20 : 0.60 : 0.20 | $Li_{11}Nd_{18}Al_4O_{38.5}$, $NdAlO_3$ and $Nd_2O_3$ |
| 8 | 0.30 : 0.40 : 0.30 | Y, $LiAlO_2$ and $NdAlO_3$ |
| 9 | 0.30 : 0.20 : 0.50 | $LiAlO_2$ and $NdAlO_3$ |
| 10 | 0.20: 0.20 : 0.60 | $LiAlO_2$, $NdAlO_3$ and $LiAl_5O_8$ |
| 11 | 0.10 : 0.10 : 0.80 | $NdAlO_3$, $LiAl_5O_8$ and $Al_2O_3$ |
| 12 ($Li_8Nd_{18}Al_5O_{38.5}$)* | 0.258 : 0.580: 0.161 | Y, $Nd_2O_3$ and $NdAlO_3$ |
| * A composition reported in the literature [4] for the phase identified here as composition 1 and labelled phase Y  \n\n**Y represents $Li_{11}Nd_{18}Al_4O_{38.5}$ | | |

Table 2. Fitted spectral parameters for room temperature Mössbauer spectrum of

$Li_{11}Sm_{18}Fe_4O_{39-\delta}$
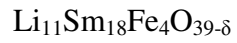
| Site | Centre Shift, $\delta$ / $\pm$ 0.02 mm s$^{-1}$ | Quadrupole Splitting, $\Delta$ / $\pm$ 0.02 mm s$^{-1}$ | HWHM Linewidth, $\Gamma/2$ / $\pm$ 0.02 mm s$^{-1}$ | Area / $\pm$ 2 % | Fit Reduced $\chi^2$ |
|---|---|---|---|---|---|
| $Fe^{4+}$ (2a) | -0.28 | 0.36 | 0.17 | 21.9 | |
| $Fe^{3+}$ (8e) | 0.29 | 0.14 | 0.18 | 67.8 | 0.554 |
| $Fe^{3+}$ (16i?) | 0.10 | 1.11 | 0.18 | 10.3 | |

**Supplementary Table 1.** Results of Rietveld refinement of $Li_{11}Nd_{18}Al_4O_{38.5}$.

| | | |
|---|---|---|
| Nd(1) 24k : 0, y, z | y | 0.30637(7) |
| | z | 0.30499(8) |
| | $U_{iso}/Å^2$ | 0.0061(1) |
| Nd(2) 12f : x, 0, 0 | x | 0.34739(7) |
| | $U_{iso}/Å^2$ | 0.0066(2) |
| Al(1) 2a : 0, 0, 0 | $U_{iso}/Å^2$ | 0.0164(10) |
| Al,Li(2) 8e : ¼,¼,¼ | occupancy Al,Li | 0.65 , 0.35 |
| | $U_{iso}/Å^2$ | 0.0066(6) |
| Al,Li(1) 16i : x, x, x | x | 0.36671(18) |
| | occupancy Al,Li | 0.05 , 0.95 |
| | $U_{iso}/Å^2$ | 0.0149(6) |
| O(1) 48l : x, y, z | x | 0.86303(7) |
| | y | 0.85850(8) |
| | z | 0.69523(5) |
| | $U_{iso}/Å^2$ | 0.0113(1) |
| O(2) 6d : ¼, ½, 0 | $U_{iso}/Å^2$ | 0.0097(3) |
| O(3) 12g : x, 0, ½ | x | 0.63110(11) |
| | $U_{iso}/Å^2$ | 0.0079(2) |
| O(4) 48l : x, y, z | x | 0.1405(5) |
| | y | 0.0269(9) |
| | z | 0.0158(34) |
| | occupancy | 0.23 |
| | $U_{ij}/Å^2$ | 0.042(2), 0.144(11),0.199(22) -0.075(5), 0.057(15), 0.007(7) |
| Li(3) 24k : x, 0, z | x | 0.1427(22) |

| | | |
|---|---|---|
| | z | 0.2092(19) |
| | occupancy | 1/6 |
| | $U_{\mathrm{iso}}/\text{Å}^2$ | 0.0234(44) |
| a(Å) | | 11.88383(10) |
| $\chi^2 = 1.648$ | $R_{\mathrm{wp}} = 1.57\%$ | $R_{\mathrm{p}} = 3.73\%$ |
| Space group | | $P\,m\overline{3}n$ |

**Supplementary Table 2.** Selected bond lengths (Å) in $Li_{11}Nd_{18}Al_4O_{38.5}$.

| | | | |
|---|---|---|---|
| Nd1-O1 | 2.611(1) × 2 | Al1-O4 | 1.710(8) × 6 |
| Nd1-O1 | 2.547(1) × 2 | 8*i*-O1 | 1.9724(5) × 6 |
| Nd1-O1 | 2.498(1) × 2 | 16*i*-O1 | 2.041(2) × 3 |
| Nd1-O2 | 2.412(1) | 16*i*-O4 | 1.89(3) × 3 |
| Nd1-O3 | 2.423(1) | Li3-O1 | 2.65(2) × 2 |
| Nd1-O3 | 3.093(1) | Li3-O1 | 2.03(1) × 2 |
| Nd2-O1 | 2.3946(6) × 4 | Li3-O4 | 2.18(2) |
| Nd2-O3 | 2.3909(11) × 2 | Li3-O4 | 1.61(3) |
| Nd2-O4 | 2.487(7) | Li3-Li1 | 1.83(1) |

**Supplementary Table 3**. Results of sample heat treatment in the $Li_2O$-$Nd_2O_3$-'CoO'

system

| Number (target formula) | Molar ratio Li :Nd: Co | Phases present |
|---|---|---|
| 1 ($Li_{11}Nd_{18}Co_4O_\delta$) | 0.333 : 0.546 : 0.121 | Y |
| 2 ($LiCoNd_4O_8$) | 0.166 : 0.667 : 0.166 | LCN4+NC |
| 3 ($Li_8Nd_{18}Co_4O_\delta$) | 0.267 : 0.600 : 0.133 | Y+ LCN4+N |
| 4 | 0.60 : 0.20 : 0.20 | Y+LC+L |
| 5 | 0.50 : 0.40 : 0.10 | Y+ LC+L |
| 6 | 0.400 : 0.514 : 0.086 | Y+LN+L |
| 7 | 0.33 : 0.58 : 0.09 | Y+LN+ N |
| 8 | 0.20 : 0.70 : 0.10 | Y+LCN4+N |
| 9 | 0.30 : 0.50 : 0.20 | Y+LCN4+LC |
| 10 | 0.10: 0.70 : 0.20 | LCN4+ NC+ Nd |
| 11 | 0.20 : 0.40 : 0.40 | LC+NC+LCN4 |
| 12 | 0.30 : 0.20 : 0.50 | LC+ NC |
| 13 | 0.258 : 0.581 : 0.161 | Y+LCN4+LC |
| 14 | 0.20 : 0.20 : 0.60 | LC+NC+C |
| 15 | 0.70 : 0.10 : 0.20 | Y+LC+L |

| 16 | 0.364 : 0.546 : 0.09 | Y+LN+N |
|---|---|---|
| 17 | 0.30 : 0.55 : 0.05 | Y+LC |
| 18 | 0.183 : 0.667 : 0.15 | Y+LC+N |
| 19 $Li_{8.1}Nd_{18}Co_4O_{37.55}$ | 0.269 : 0.598 : 0.133 | Y solid solution |
| 20 $Li_{8.52}Nd_{18}Co_4O_{37.76}$ | 0.279 : 0.590 : 0.131 | Y solid solution |
| 21 $Li_{8.93}Nd_{18}Co_4O_{37.97}$ | 0.289 : 0.582 : 0.129 | Y solidsolution |
| **Y:** $Li_{11}Nd_{18}Co_4O_{39-\delta}$, LCN4: $LiCoNd_4O_8$, NC: $NdCoO_3$, LC: $LiCoO_2$, LN: $LiNdO_2$, N: $Nd_2O_3$, C: 'CoO', L: $Li_2O$, Y solid solution: $Li_{11-X}Nd_{18}Co_4O_{39-0.5X}$ (x=0 - ~2.9). | | |

Figure 1



$Al_2O_3$

1 : $Li_{11}Nd_{18}Al_4O_{38.5}$
12 : $Li_8Nd_{18}Al_5O_{38.5}$

$LiAl_5O_8$

○ 11

○ 10

$LiAlO_2$       9 ○       $NdAlO_3$

○ 8

6 ○    ○ 7

$Li_5AlO_4$    ○ 5    ○ 12

1

4 ○

3 ○    ○ 2

$Li_2O$                                $Nd_2O_3$

$LiNdO_2$

Figure 2

Figure 3



1: $Li_{11}Nd_{18}Co_4O_{39-\delta}$
2: $LiCoNd_4O_8$
3: $Li_8Nd_{18}Co_4O_{39}$

Supplementary Figure 1

**(a)**



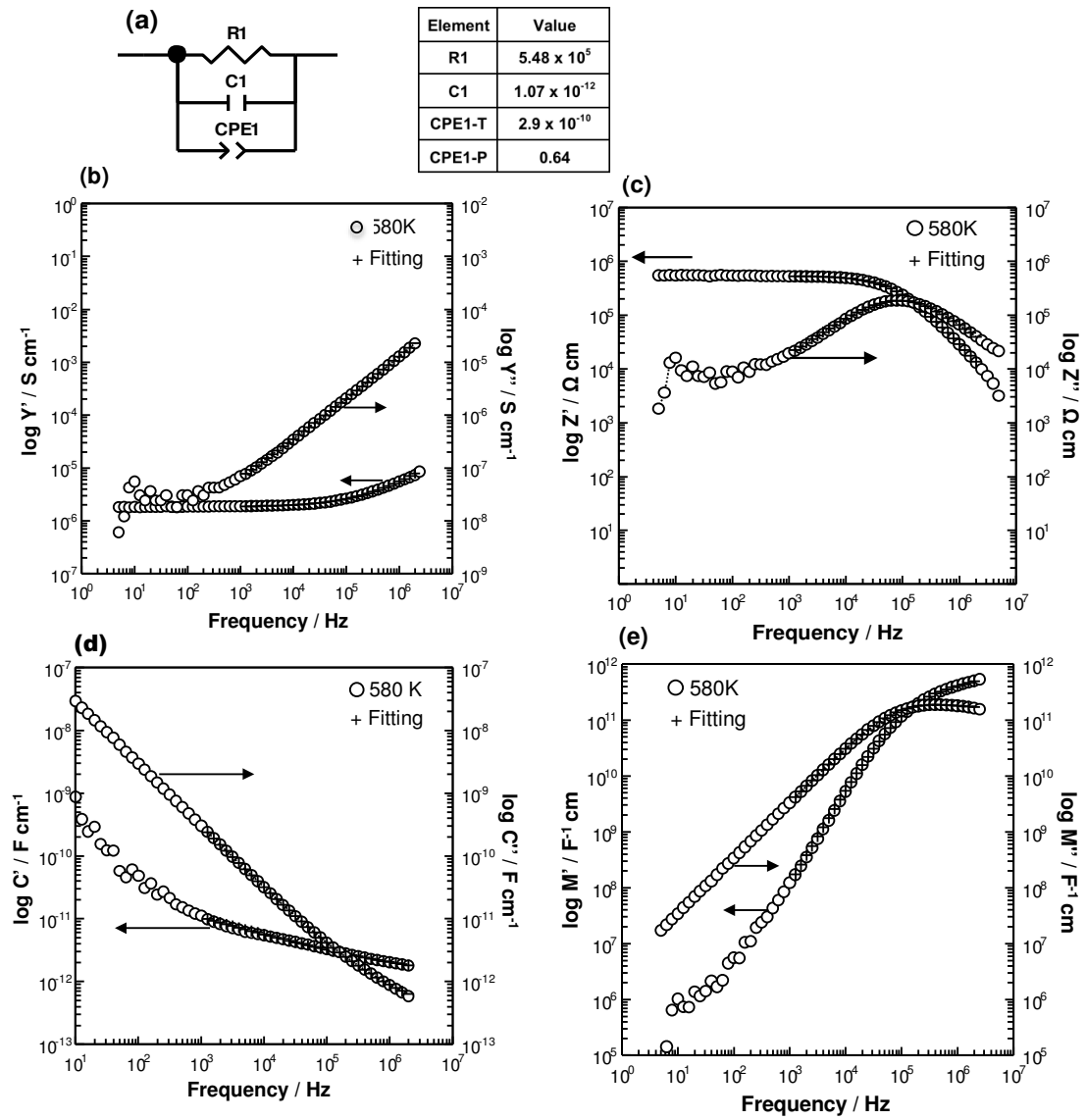$Li_{11-x}Nd_{18}Co_4O_{39-\delta}$

X=2.90

X=2.48

X=2.07

X=0

**(b)**



X=2.90

X=2.48

X=0
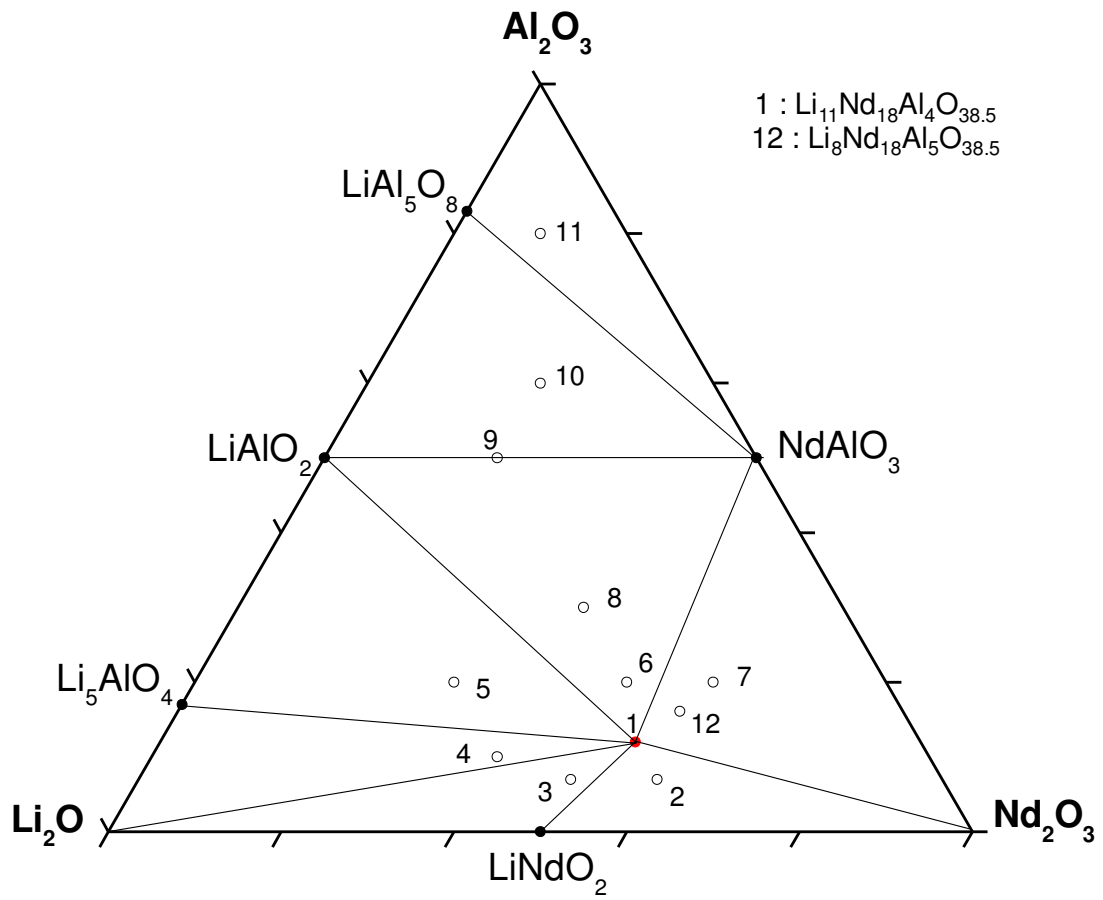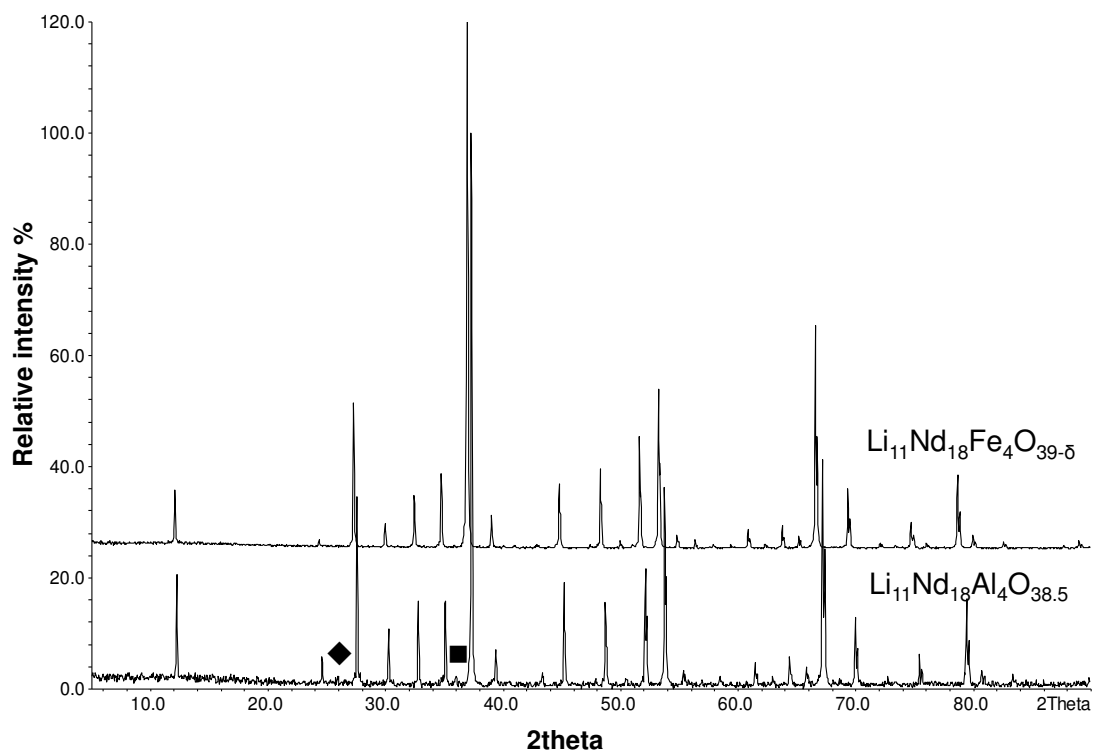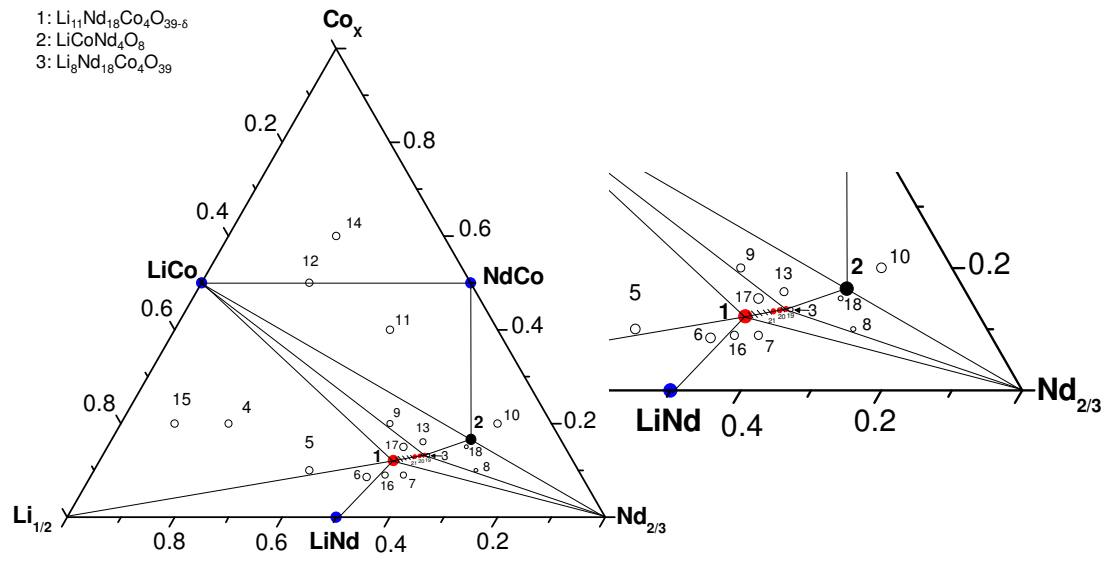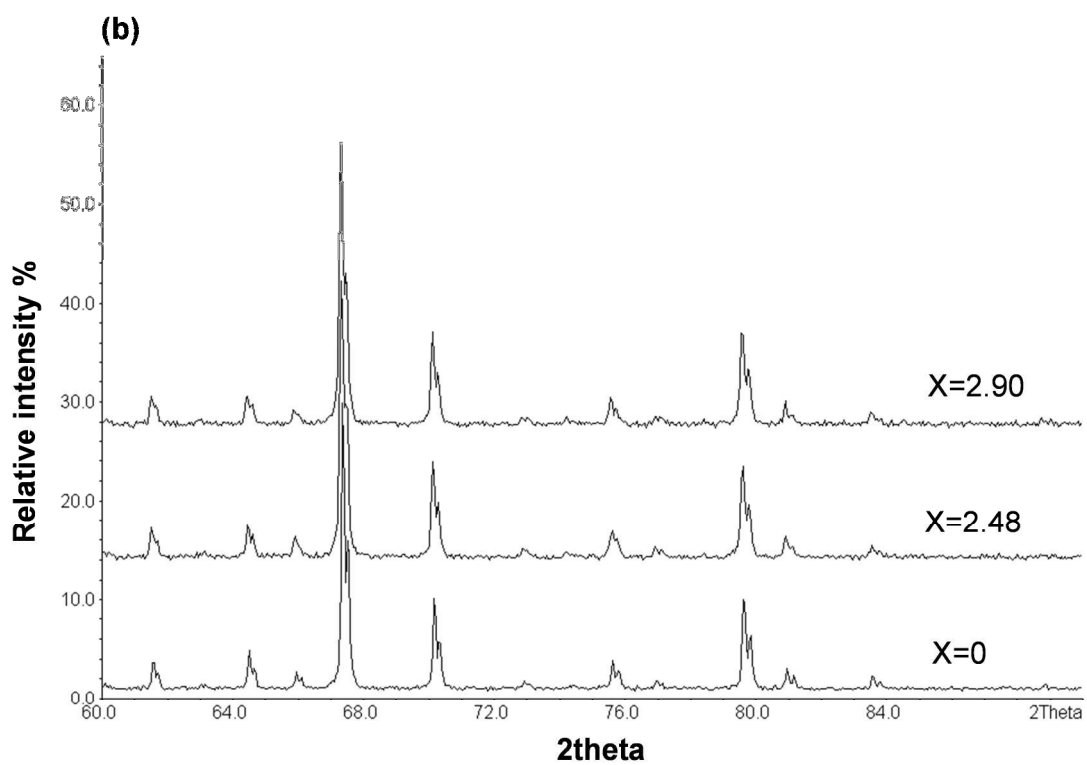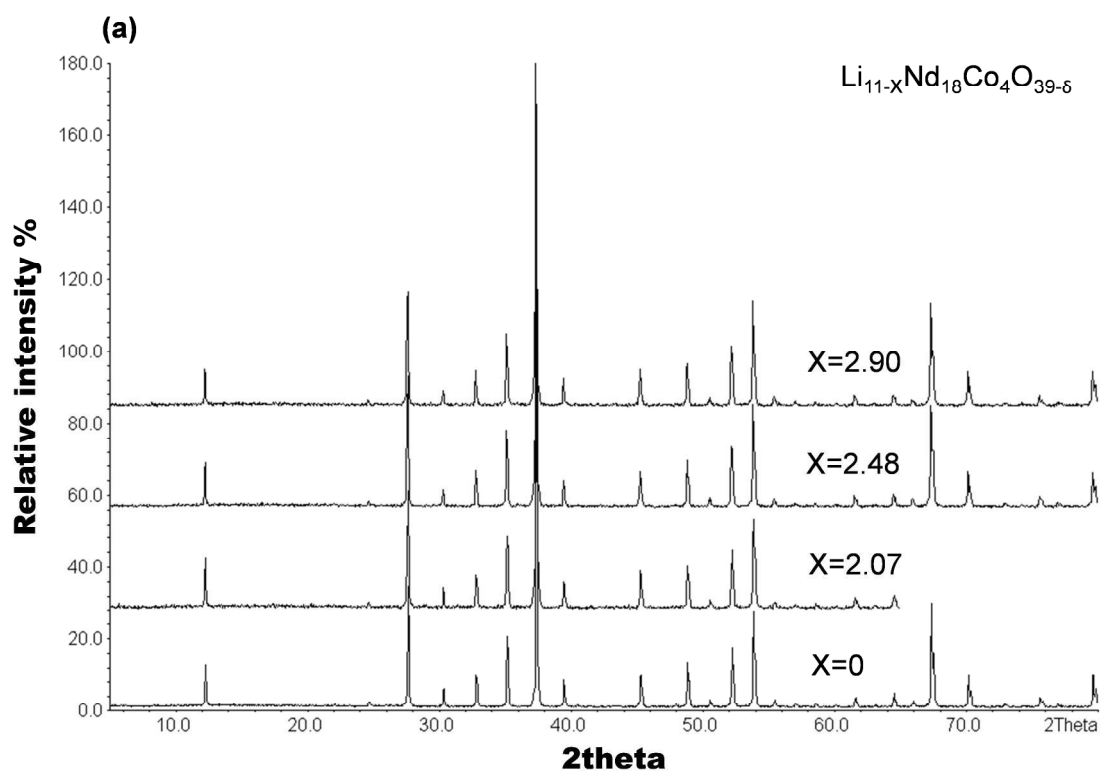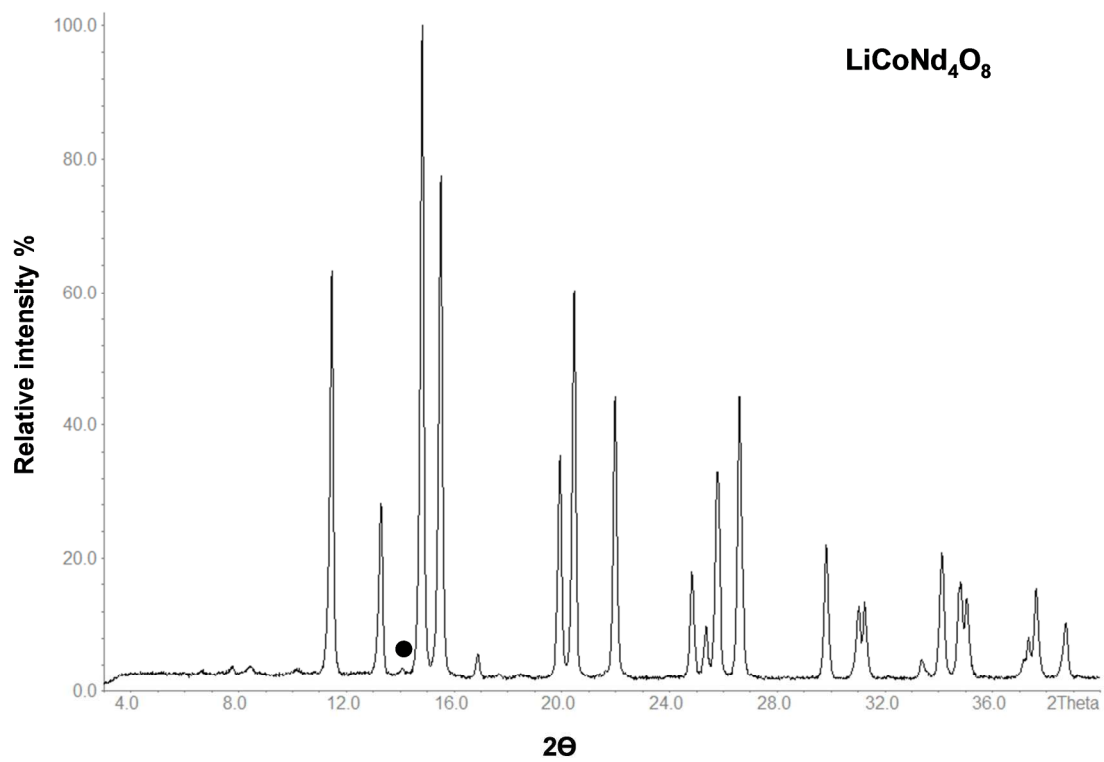
Figure 4

Supplementary Figure 2



Figure: XRD patterns with Relative intensity % (y-axis) versus 2theta (x-axis) for $Li_{11}Sm_{18}Co_4O_{39-\delta}$, $Li_{11}Sm_{18}Fe_4O_{39-\delta}$, $Li_{11}Nd_{18}Co_4O_{39-\delta}$, and $Li_{11}Nd_{18}Fe_4O_{39-\delta}$.
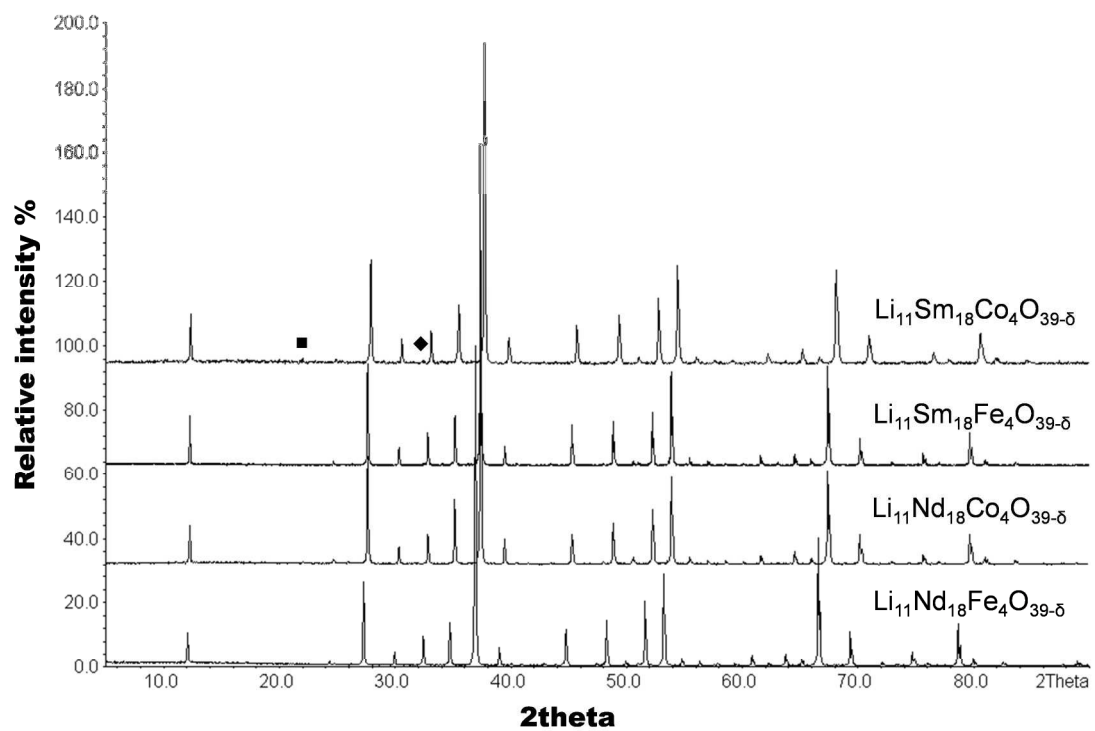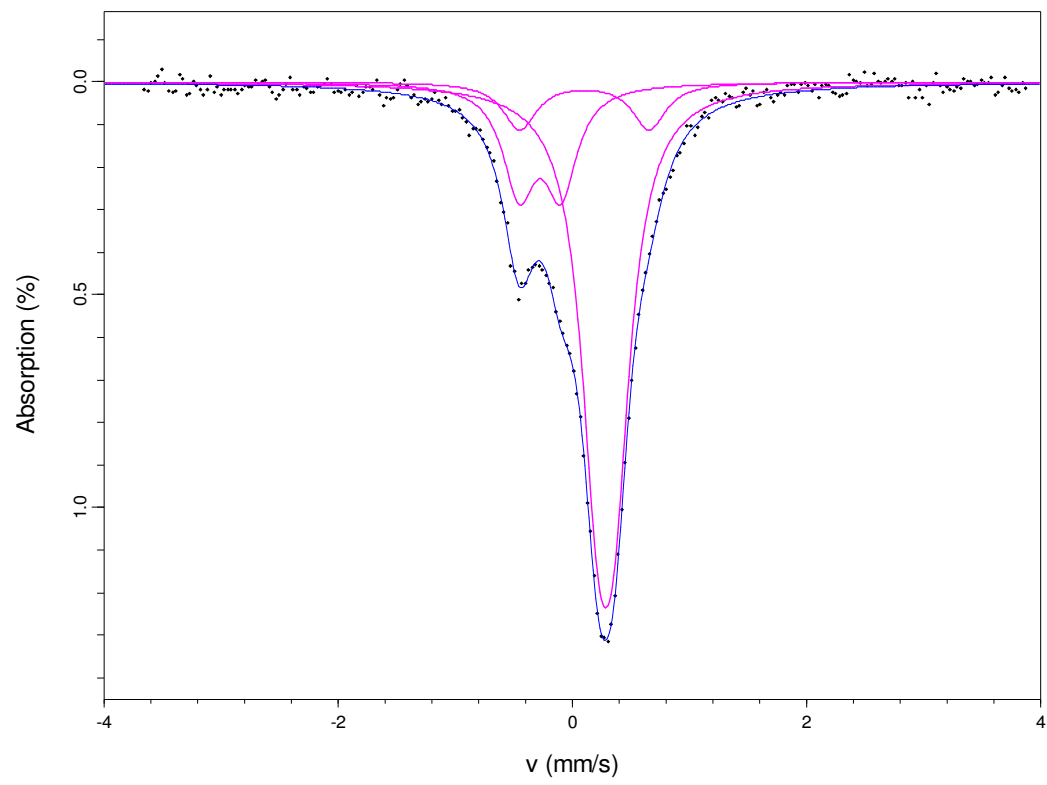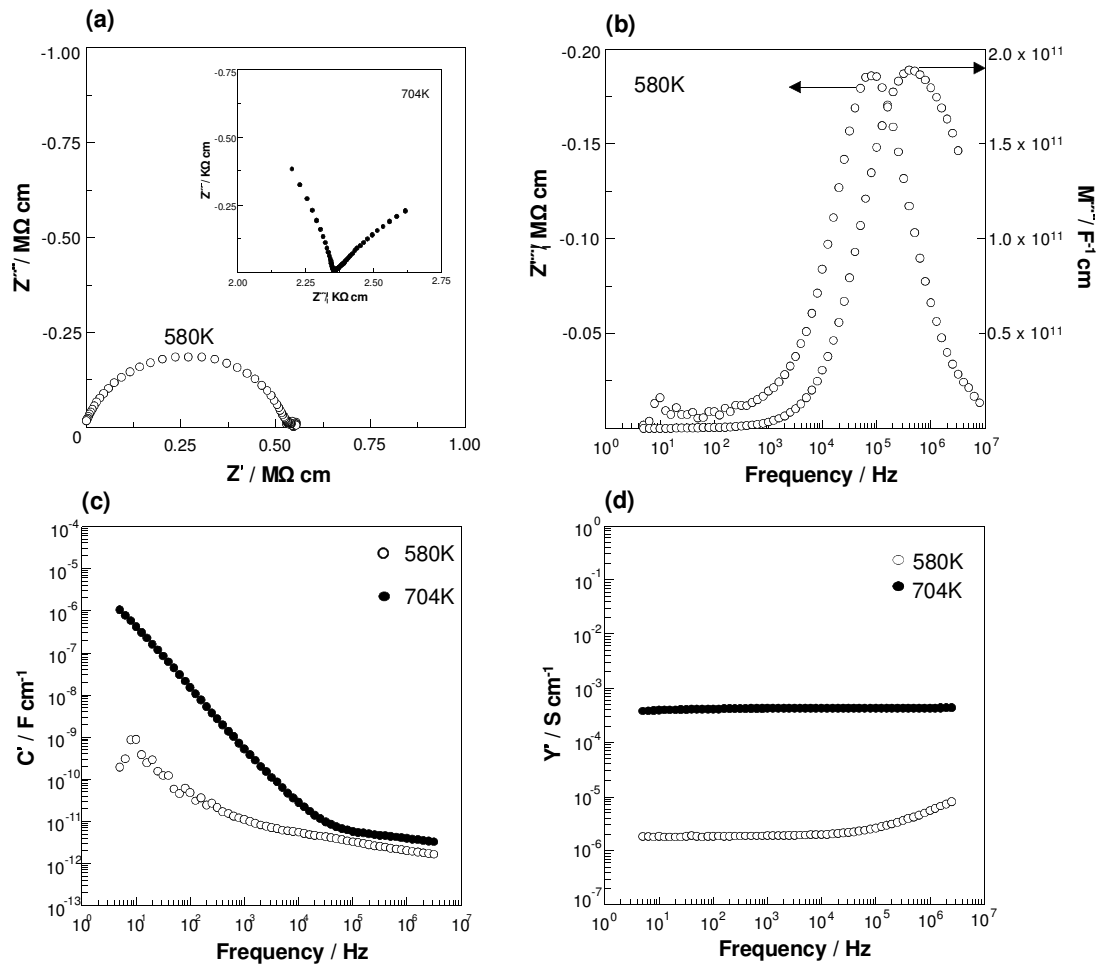
Figure 5

Figure 6

Figure 7

Figure 8
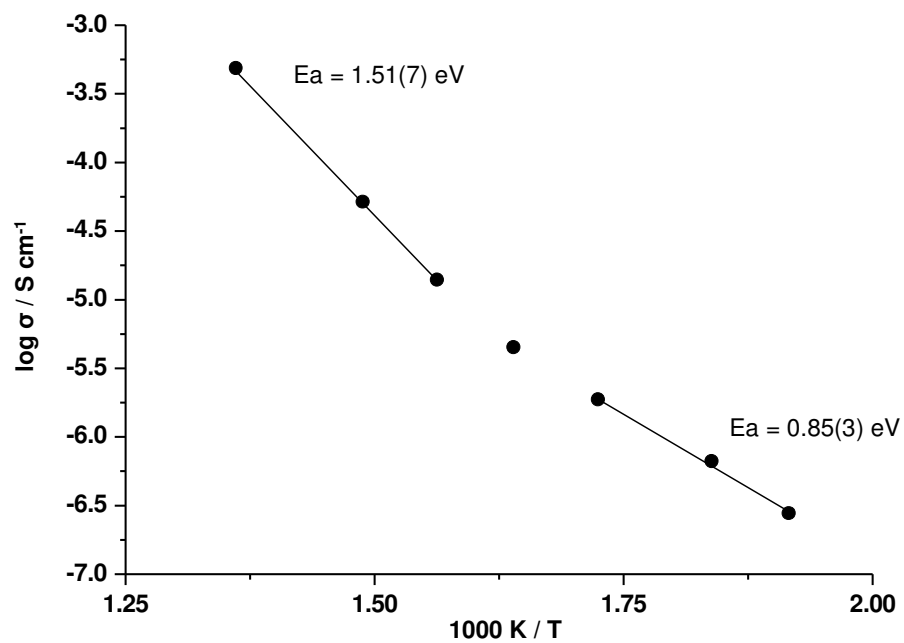
Supplementary Figure 3

Figure 9



(a)

$Li_{11-x}Nd_{18}Co_4O_{39-\delta}$
- X=0, Ea=0.33(2) eV
- X=2.90, Ea=0.31(8) eV
- X=2.48, Ea=0.29(5) eV
- X=2.07, Ea=0.28(9) eV
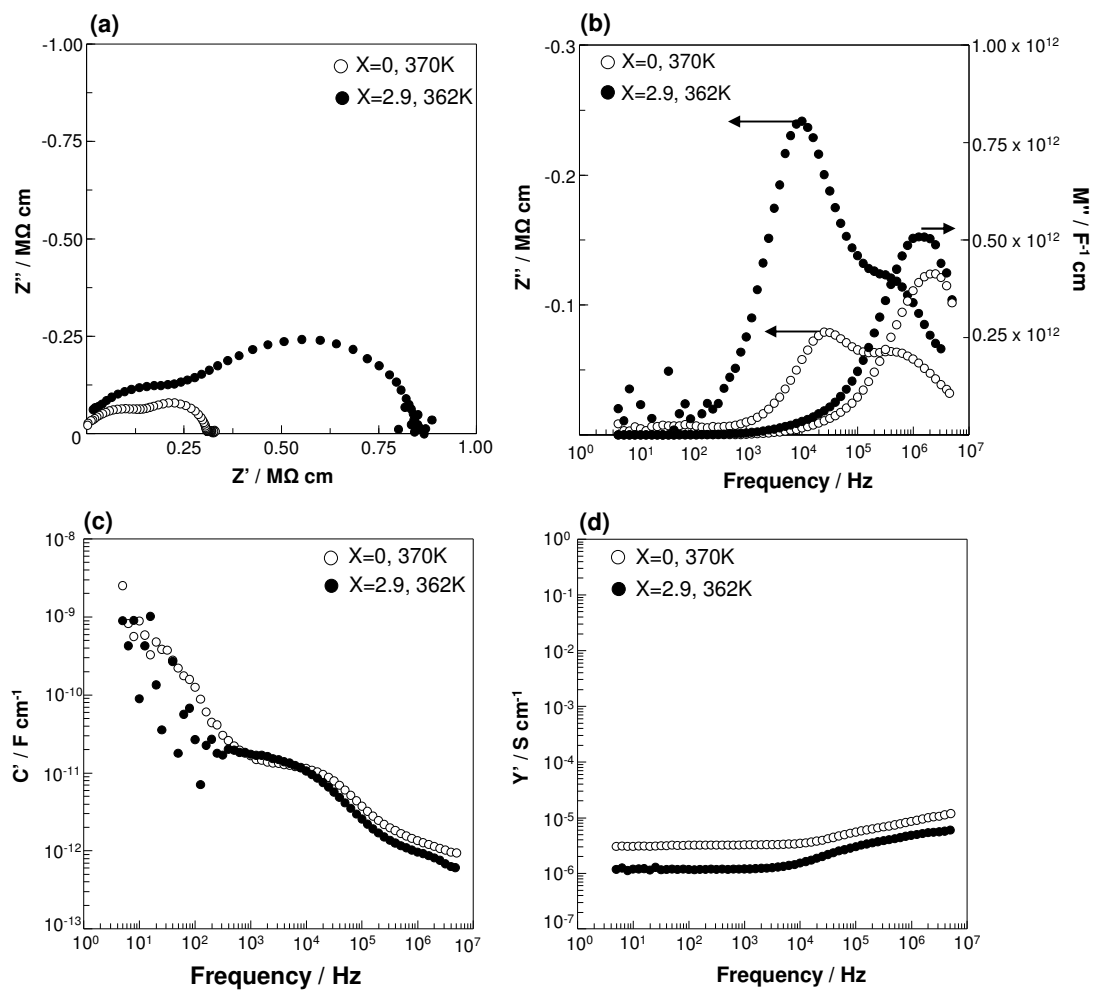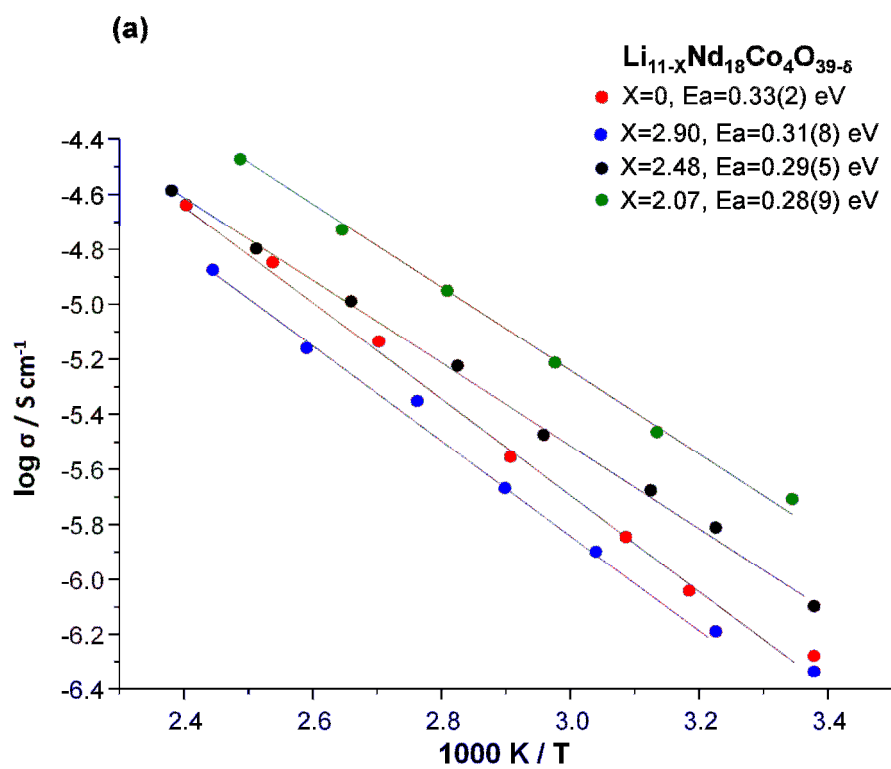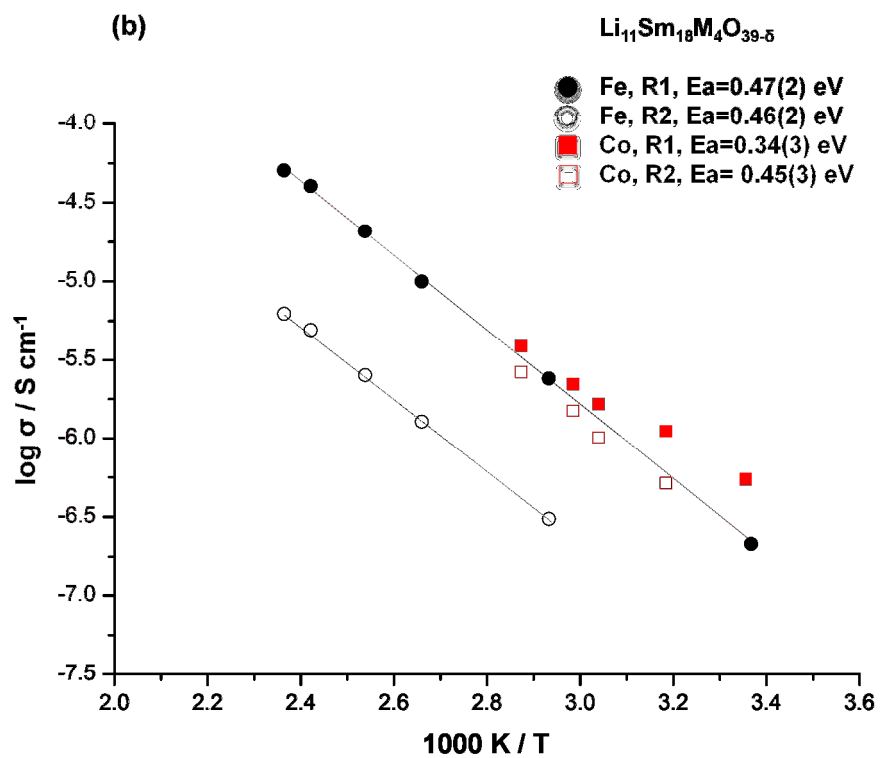
Figure 10

References

(1) Mazza, D.; Abbatista, F.; Vallino, M.; Ivaldi, G. J. Less-Common Met., 1985, **106** (2), 277−285.

(2) Ban, I.; Drofenik, M.; Suvorov, D.; Makovec, D. Mater. Res. Bull., 2005, **40** (10), 1856−1863.

(3) Frampton, P. P. C.; Battle, P. D.; Ritter, C. Inorg. Chem. 2005, **44** (20), 7138−7142.

(4) Drofenik, M.; Ban, I.; Makovec, D.; Hanzel, D.; Golobic, A.; Golic, L. J. Solid State Chem. 2007, **180** (1), 2−7.

(5) Dutton, S. E.; Battle, P. D.; Grandjean, F.; Long, G. J.; Oh-ishi, K. Inorg. Chem. 2008**, 47** (23), 11212−11222.

(6) Dutton, S. E.; Battle, P. D.; Grandjean, F.; Long, G. J.; van Daesdonk, P. A. Inorg. Chem. 2009, **48** (4), 1613−1623.

(7) Battle, P. D.; Dutton, S. E.; van Daesdonk, P. A. J. Solid State Chem. 2010, **183** (7), 1620−1624.

(8) Battle, P. D.; Dutton, S. E.; Thammajak, N.; Grandjean, F.; Sougrati, M. T.; Long, G. J.; Oh-ishi, K.; Nakanishi, S. Inorg. Chem. 2010, **49** (13), 5912−5922.

(9) Battle, P. D.; Dutton, S. E.; Grandjean, F.; Long, G. J.; Thammajak, N.; Wisetsuwannaphum, S. J. Solid State Chem. 2011, 184 (9), 2580−2587.

(10) Chen, Y-C.; Reeves-McLaren, N.; Bingham, P.A.; Forder, S.D.; West, A.R. Inorg. Chem. 2012, **51**, 8073-8082.

(11) Varez, A.; Fernández-Díaz, M.T.; Alonso, J.A.; Sanz, J. Chem. Mater. 2005, **17**, 2404-2412.

(12) Truong, L.; Howard, M.; Clemens, O.; Knight, K.S.; Slater, P.R.; Thangadurai, V. J. Mater. Chem. A. 2013, **1**(43), 13469-13475.

(13) Irvine, J.T.S.; Sinclair, D.C.; West, A.R.; Adv. Mater.; (1990), **2**, 132-138.

(14) Jonscher, A.K.; Dielectric Relaxation in Solids, Chelsea Dielectrics Press, London, 1983.

(15) Bruce, P.G.; West, A.R.; J. Electrochem. Soc.; (1982), **130**, 662-669.

(16) Thammajak, N.; Battle, P.D.; Brown, C.; Higgon, K.; Stansfield, R.; J. Solid State Chem.;2014**,  209,** 120-126.